Effects of Combined Mode Loadings on Fracture and Flaw Growth

Ramesh C. Shah*
Boeing Aerospace Co., Seattle, Wash.

An experimental investigation was conducted to determine the effects of combined mode loading on crack instability and cyclic flaw growth characteristics in the presence of the opening, sliding, and tearing modes of crack extension. Surface flawed cylindrical specimens of 2219-T87 aluminum and 6A1-4V βSTA titanium were tested under tension and/or torsion loading. For this specific specimen-crack geometry configuration, results show that an applied tearing mode stress intensity factor K_{III} less than 70% of K_{IIIcr} has little effect on the opening mode stress intensity factor K_I at which fracture occurs. Similarly, the application of K_I up to about 70% of K_{Icr} has little effect on the K_{III} at which fracture occurs. These results are compared with the results of other investigators obtained for different materials. The lower bound of fracture criterion under combined Mode I-III loading is given by the equation $(K_I/K_{Icr})^2 + (K_{III}/K_{IIIcr})^2 = 1$. Cyclic lives for surface flawed cylindrical specimens subjected to combined tension and torsion can be reasonably predicted from the cyclic lives of the surface flawed specimens subjected to pure tension and the static fracture criterion for the same flaw-specimen configuration under combined tension and torsion.

Introduction

THE majority of past experimental and theoretical fracture and crack growth studies have dealt with the opening mode of crack surface deformation (Mode *I*) conditions. Many investigations have shown that under Mode I conditions, crack instability occurs when the stress intensity factor reaches some critical value. Extensive investigations have also been carried out to determine fatigue crack growth rates and fatigue lives for cracked components subjected to opening mode crack deformations. However, under service conditions cracked components may be loaded so that all the three modes (opening, sliding, and tearing) or more than one mode of crack surface displacements are present, such as at cracks located in regions where tensile and shear stresses exist simultaneously. This could happen even in a cracked structure loaded in uniaxial tension if the crack is inclined with respect to loading direction. Despite its practical importance, a very limited number of theoretical and experimental investigations have been conducted to determine the effects of combined mode loadings on fracture starting from cracks.[1-11]

For a cracked component under combined mode loading, two theories of fracture have been advanced, namely, maximum stress criterion[1] and strain energy density factor theory.[8,9] Earlier experimental studies include the effects of Mode I-II interaction on plexiglass,[1] balsa wood,[2] fiberglass,[2] 2000 and 7000 series aluminum alloys[3-7] and 4340 steel,[11] and Mode I-III interaction on 7000 series aluminum alloys,[4,5] K9 tool steel,[5] and 4340 steel,[11] and Mode I-II-III interaction on 4340 steel.[11] Very little published information exists to date on crack propagation rates under the combined loadings of opening and sliding modes.[3] To the author's knowledge, no information exists on cyclic flaw growth in the presence of Modes I and III (opening and tearing modes of crack surface displacements) or combined Modes I-II-III (opening, sliding, and tearing modes).

The present experimental investigation was conducted to determine the effects of combined Modes I-II-III on fracture and cyclic flaw growth in 2219-T87 aluminum and 6A1-4V βSTA titanium alloys. For tension-loaded surface flawed cylindrical specimens, only Mode I stress intensity factor (K_I) exists. As shown from the results of three-dimensional photoelastic tests, K_I is maximum at the maximum flaw depth and is minimum at the intersection of the flaw periphery and the specimen boundary for the flaw shapes tested.[12] For torsion-loaded surface flawed cylindrical specimens, K_{II} is minimum and is negligibly small at the maximum crack depth. K_{II}, however, is maximum at the intersection of the flaw periphery and the specimen boundary.[12] K_{III} is maximum at the maximum crack depth and is small near the intersection of the flaw periphery and the specimen boundary. Thus, the flaw peripheries of the surface flawed cylindrical specimens subjected to combined tension and torsion loadings are subjected to continuously varying values of K_I, K_{II}, and K_{III} and the flaw periphery near the maximum flaw depth is mainly subjected to K_I and K_{III} only. Surface flawed cylindrical specimens were fractured under tension and/or torsion loading to determine the failure criterion in the presence of all three modes of crack extension. Surface flawed cylindrical specimens were subjected to synchronous cyclic tensile and torsional loadings to determine cyclic flaw growth characteristics in the presence of K_I, K_{II}, and K_{III}.

Materials and Experimental Procedures

A 2.5-in. thick plate of 2219-T87 aluminum and a 1.0-in. thick plate of 6A1-4V βSTA titanium were used in the present investigation. Titanium plate was purchased in the annealed condition per MIL-T-9046F, Type III, Composition C. The plate was beta annealed (1900F for 25 min and air cooled) and then was solution treated and aged (STA) per BAC 5613. The condition III specifications are: solution treat—1725°F, 25 min, water quench; and age—1000°F, 4-5 hr, air cool.

Mechanical properties for aluminum and βSTA titanium at room temperature are given in Table 1. Chemical compositions for these materials are given in Ref. 12.

Fracture toughness K_{IE}, as determined from surface flawed flat specimens, for the aluminum in the crack propagation

Presented as Paper 74-414 at the AIAA/ASME/SAE 15th Structures, Structural Dynamics and Materials Conference, Las Vegas, Nevada, April 17-19, 1974; submitted April 29, 1974; revision received March 3, 1975. This work was supported by NASA Lewis Research Center through Contract NAS3-14346. The author wishes to express his appreciation to G. T. Smith, NASA Langley Research Center, for his interest and support. The author wishes to thank A. A. Ottlyk for conducting tests and L. R. Hall, J. N. Masters, and A. S. Kobayashi for helpful discussions.

Index categories: Materials, Properties of; Structural Design, Optimal; Structural Static Analysis.

*Senior Specialist Engineer, Research and Engineering Division.

Table 1 Mechanical properties

Material	Loading direction	0.2% offset yield strength (ksi)	Ultimate tensile strength (ksi)	Elongation in 2 in. (%)	Reduction in area (%)
2219-T87	L	57	69	12	23
Aluminum	T	55	69	10	15
6A1-4V βSTA	L	146	159	8	9
Titanium	T	146	162	8	9

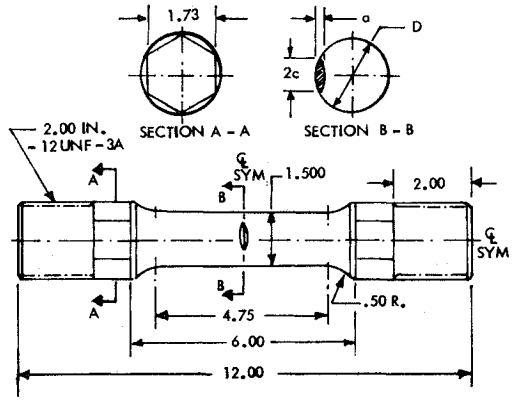

Fig. 1 Surface flawed cylindrical specimen of 2219-T87 aluminum.

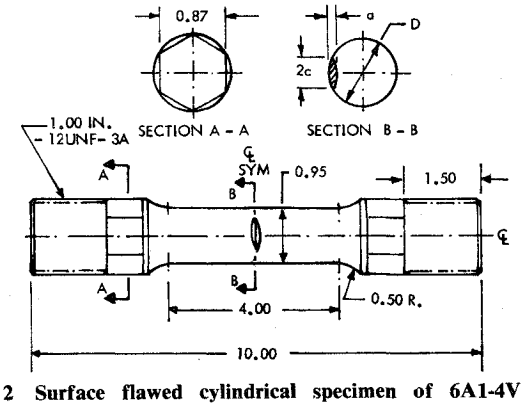

Fig. 2 Surface flawed cylindrical specimen of 6A1-4V βSTA titanium.

direction of TS and for the titanium in the crack propagation direction of LS were 36.1 and 69.2 ksi (in.) $^{1/2}$, respectively.

Specimen Preparation

Specimens of aluminum and titanium were fabricated according to Figs. 1 and 2, respectively. Starter slots with dimensions slightly less than the required final flaw dimensions were introduced in the specimens using electrical discharge machine (EDM). Starter slots were part circular. All specimens were precracked by growing fatigue cracks from EDM slots under low stress tension fatigue loadings. The maximum cyclic stress levels used were 8-10 ksi for aluminum specimens and 25-31.5 ksi for titanium specimens. Crack propagation directions for aluminum and titanium specimens were TS and LS, respectively.

Test Machine and Instrumentation

Specimens were loaded in a 150-kip capacity tension-compression machine that was modified to apply simultaneous tensile and torsional loading. The specimen was loaded in tension by a vertical hydraulic cylinder, and torque was applied independently using two horizontal hydraulic cylinders. At the lower end, the load cell was locked against any torsional motion. Axial load was measured and controlled by two independent four-arm strain-gage bridge circuits installed in the axial direction, and torque was measured and controlled by two independent four-arm strain-gage bridge circuits installed at 45° angles with respect to the axial direction. The hydraulic cylinders were actuated by servo valves responding to electrical signals to apply the programed load. The required ratio of tension to torque was maintained by a drum programmer.

For all static and cyclic specimens, axial and angular displacements across the flawed cross section were continuously measured with electrical displacement indicators. Load vs displacement curves were generated independently for axial and angular displacement by $X-Y$ plotters. Crack opening displacement in the axial direction was measured by a clip gage, shown in Fig. 3. The average output of the two displacement indicators was used to generate the load-displacement curves. Angular displacements were measured by the relative motion of two clamps located 1-in. apart, as shown in Fig. 3. Knife edges were machined at the end of arms that extended from the clamps to hold a clip gage for angular displacement measurement. The knife edges were located 1-in. away from the vertical centerline of the specimen.

Test Program and Procedures

Twenty-eight specimens of aluminum and 28 specimens of titanium were loaded to failure in an ambient environment under tension and/or torsion loading according to the test program outlined in Table 2. Flaw depth a and length 2c are defined in Figs. 1 and 2. Flaw configurations ($a/2c$ and a/D) and loading combinations are described in Table 2. As seen from Table 2, a few specimens were axially loaded to predefined tensile stress levels and then were torqued to

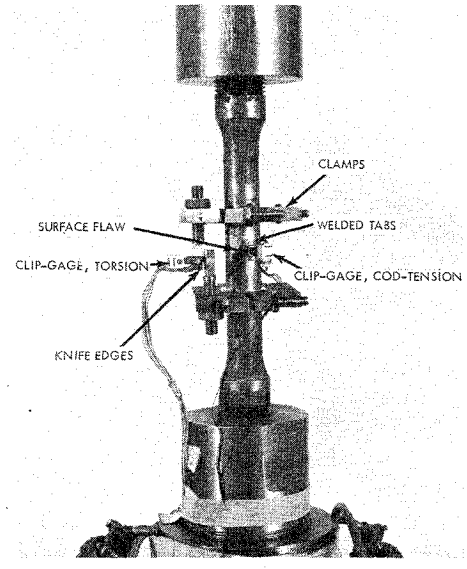

Fig. 3 Instrumentation for round specimens containing surface flaws.

Table 2 Test program for static fracture specimens

Material	Flaw depth, a (in.)	$a/2c$	a/D	Number of Static Fracture Tests in: Tension alone	Torque alone	Tension first and torqued to fracture	Torque first and failed in tension	Simultaneous tension and torsion applied
2219-T87	0.44	0.4	0.3	3	1	4	4	...
Aluminum	0.30	0.3	0.2	3	...	4	5	...
	0.26	0.36	0.2	1	...	1	1	1
6A1-4V βSTA	0.2	0.4	0.3	3	1	5	4	1
Titanium	0.19	0.3	0.2	3	1	4	5	1

Table 3 Test program for cyclic specimens

Material	Flaw depth, a (in.)	$a/2c$	a/D	$\sigma_{TENSION}$ τ_{SHEAR}	Number of Tests
2219-T87	0.29	0.3	0.2	1:0	3
Aluminum				1:1	5
				0:1	1
	0.42	0.4	0.3	1:0	3
				1:1	4
				0:1	2
6A1-4V βSTA	0.19	0.4	0.2	1:0	3
Titanium				2:1	2
				1:1	3
				0:1	1
	0.28	0.4	0.3	1:0	3
				2:1	2
				1:1	3
				0:1	1

failure while maintaining the applied tensile load. Some specimens were torqued to predefined shear stress levels and then were pulled to failure while maintaining the applied torque. A few specimens were loaded to failure under simultaneous applied tension and torsion loading.

Eighteen specimens of aluminum and 18 specimens of titanium were cycled to failure in an ambient room air environment under synchronously applied tension and torsion loadings. Experimental parameters for the flaw configuration and loading are described in Table 3.

Cyclic stress ratio (minimum cyclic stress to maximum cyclic stress) was 0.05 for tension fatigue cycles and 0.0 for shear fatigue cycles. Cyclic frequency was 20 cpm for all specimens. All aluminum and titantium specimens were cycled until either fracture occurred or fracture was imminent. Normally, a cyclic test could be terminated within a few cycles of specimen failure by observing crack opening displacement (CCD) output for the tension-loaded specimens and angular displacement output for the torsion-loaded specimens. The tests were terminated just prior to failure so that flaw peripheries could be marked and seen after pulling them to failure in tension.

Test Results and Discussion

Static Fracture Tests

Detailed test results of static fracture tests of 56 aluminum and titanium specimens are presented in Ref. 12. These specimens were loaded to failure at room temperature in combined tension and torsion loadings. Failure stresses σ_F and τ_F, mentioned hereafter, were calculated from the fracture load P_F and the fracture torque T_F as follows

$$\sigma_F = 4P_F/(\pi D^2) \qquad \tau_F = 16T_F/(\pi D^3) \tag{1}$$

Shear stress τ_F, thus, is the maximum gross shear stress at the surface of the cylindrical specimen.

Typical plots of crack opening displacement in the axial direction vs tensile load and angular displacement across the crack plane vs torque are shown in Fig. 4. Figure 4 shows these plots for 4 aluminum specimens subjected to different ratios of tension stress at failure to shear stress at failure, σ_F/τ_F. These specimens had flaws of dimension $a \approx 0.44$ in. and $2c \approx 1.15$ in. Behavior of COD vs tensile load and angular displacement vs torque for titanium specimens and specimens with other sizes at a given σ_F/τ_F ratio was similar to that of these specimens for the corresponding σ_F/τ_F ratio. Specimen 1A1-12 (Fig. 4) was subjected to a tensile load of 41.1 kips. COD vs load behavior was linear. The specimen was then subjected to torsion while maintaining the tensile load. As the torque was applied COD remained constant initially and then started to increase, as shown in Fig. 4. Specimen 1A1-3 was subjected to a torque to 20,300 in.-lb. While maintaining this torque constant, the specimen was subjected to tensile load. The angular displacement remained constant initially and then started to increase with increasing load. Nonlinear behavior of the displacement for these two specimens can be due to any or all of the following factors: 1) plastic yielding around the flaw periphery, 2) warping of the flawed cross section, and 3) flaw growth. The possibility of flaw growth could not be ruled out since none of these specimens were unloaded and subjected to low stress fatigue cycles to mark the flaw peripheries. Specimen 1A1-10 was failed in pure torsion. The gross maximum shear stress at the surface of the specimen was 36.1 ksi, which is about 10% higher than the calculated shear yield strength of the material, τ_{ys}. (τ_{ys} was not measured. It was assumed to be equal to the tensile yield stress divided by $\sqrt{3}$ from Mise's yield condition.)

Good estimates for the stress intensity factors for the surface flawed cylindrical specimens subjected to tension or torsion are not available. As previously mentioned, results of 3-dimensional photoelastic tests gave the variations of K_I or K_{II} around the flaw periphery for specimens subjected to tension or torsion, respectively.[12] For tension-loaded flawed

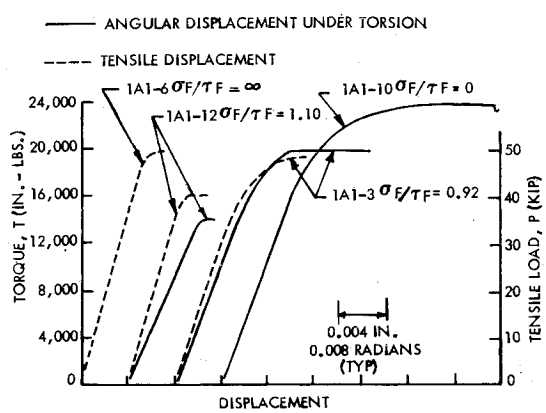

Fig. 4 Load-displacement records for aluminum specimens subjected to tension and torsion ($a \approx 0.44$ in., $2c \approx 1.15$ in.).

specimens, upper and lower bound of stress intensity factor K_I can be established and K_I can be calculated within 15% error. For torsion-loaded specimens, K_{II} can be calculated from photoelastic results of Ref. 12 but K_{III} could not be. Since flaw dimensions do not vary more than 5% between specimens for a group of specimens of a material, the fracture results are plotted and compared in terms of tensile stress at failure σ_F vs shear stress at failure τ_F in Figs. 5-8. Figures 5 and 6 show the plots of σ_F vs τ_F for aluminum specimens containing flaws of dimensions a and $2c$ approximately equal to either 0.44 in. and 1.15 in. or 0.30 in. and 0.98, respectively.

Figures 7 and 8 show similar plots for titanium specimens containing flaws of dimensions a and $2c$ approximately equal to either 0.28 in. and 0.68 in. or 0.19 in. and 0.61 in., respectively. Failure stress τ_F in pure shear ($\sigma_F=0$) in Fig. 6 was estimated as 40.4 ksi.[12] Probable failure criterion under combined loading for each flaw size is also shown in these plots. In the following, σ_c is defined as the failure stress σ_F for a flawed specimen subjected to pure tension only ($\tau_F=0$). τ_c is defined as the failure stress τ_F for a flawed specimen subjected to pure tension only ($\sigma_F=0$).

Results in Figs. 5-8 show that the presence of shear stress τ_F up to about 0.7 τ_c has little effect (less than 0.2 σ_c) on tensile stress σ_F at which fracture occurs. Results in Fig. 5 and 6 of aluminum specimens show that for the same flaw size and applied shear stress of approximately 30 ksi, if torque was applied prior to applying tension load, the specimen required higher tensile load to fail than when tensile load was applied prior to torsion. Results in Figs. 7 and 8 of titanium specimens show that for constant values of flaw size and applied torque, if torque is applied prior to applying tensile load, slightly higher tensile failure loads are obtained than when the tensile load is applied prior to torsion.

The later observations may be explained as follows. When high shear stress is applied first, crack surfaces may overlap due to twisting and the crack may blunt due to yielding. Subsequently, when tensile load is applied, the crack would not open up as much as when tensile load is applied first. As a result, the specimen would require higher tensile load to fail when it is first subjected to high shear stress.

Figure 9 shows fracture surfaces for six titanium specimens subjected to different ratios of σ_F/τ_F. These specimens contained flaws of dimensions $a\approx0.28$ in. and $2c\approx0.68$ in. Fracture surfaces of other titanium and aluminum specimens for the corresponding σ_F/τ_F ratios were similar to fracture surfaces of these specimens. The specimen subjected to pure tension ($\sigma_F/\tau_F=\infty$) had a flat fracture with slight shear lips at the periphery of the specimen. The specimen subjected to pure torsion ($\sigma_F/\tau_F=0$) had a flat fracture with shear rubbing marks over the fracture surface. Specimens subjected to tension and torsion had antisymmetric fracture surfaces, as shown in Fig. 9. Fracture surfaces of specimens subjected to $\sigma_F/\tau_F=2.28$ and 1.10 had textures similar to that of the pure tension specimen. Some shear rubbing marks were visible on the fracture surface of the specimen subjected to $\sigma_F/\tau_F=1.10$. Fractures for these specimens appeard to be controlled by Mode I. Fracture surfaces of specimens subjected to $\sigma_F/\tau_F=0.58$ and 0.30 had shear rubbing marks over the entire surface similar to the fracture surface of the pure torsion specimen.

Careful examination of fracture surfaces of the specimens indicated that the fracture originated at the area near the point of maximum crack depth for most specimens. Fracture origin for some specimens, where torsion was applied prior to tensile load, could not be identified positively. As mentioned before, stress intensity factor K_I and K_{III} are maximum at the maximum crack depth, and K_{II} is nearly zero there for the specimens subjected to combined tension and torsion. Also, the constraint to the crack tip deformation is maximum there. Thus, it seems that for this specimen-loading configuration, the fracture originated mainly under combined Mode I-III conditions even though other points on the flaw periphery

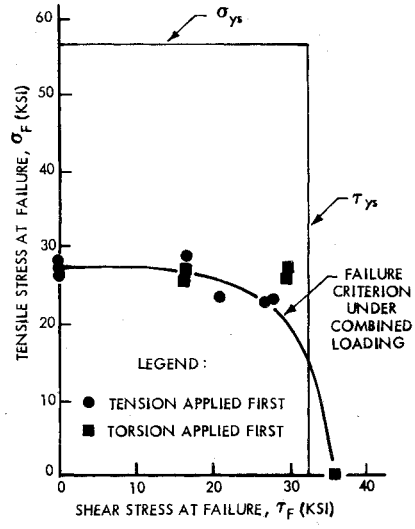

Fig. 5 Fracture results of aluminum specimens subjected to tension and torsion ($a\approx0.44$ in., $2c\approx1.15$ in.).

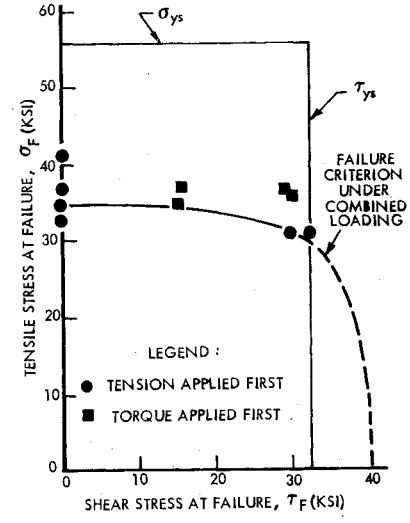

Fig. 6 Fracture results of aluminum specimens subjected to tension and torsion ($a\approx0.30$ in., $2c\approx0.98$ in.).

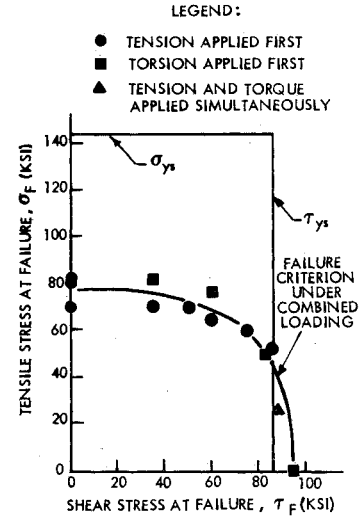

Fig. 7 Fracture results of titanium specimens subjected to tension and torsion ($a\approx0.28$ in., $2c\approx0.68$ in.).

were subjected to all three modes of crack surface displacements. As described in Ref. 11, the ratios of K_I/K_{Icr} and K_{III}/K_{IIIcr} can be calculated by Eq. (2) with little error from the failure stresses σ_F and τ_F of the combined tension and torsion specimens and the failure stresses σ_c and τ_c for the identical flawed specimens subjected to pure tension or torsion, respectively.

$$K_I/K_{Icr}=\sigma_F/\sigma_c \text{ and } K_{III}/K_{IIIcr}=\tau_F/\tau_c \qquad (2)$$

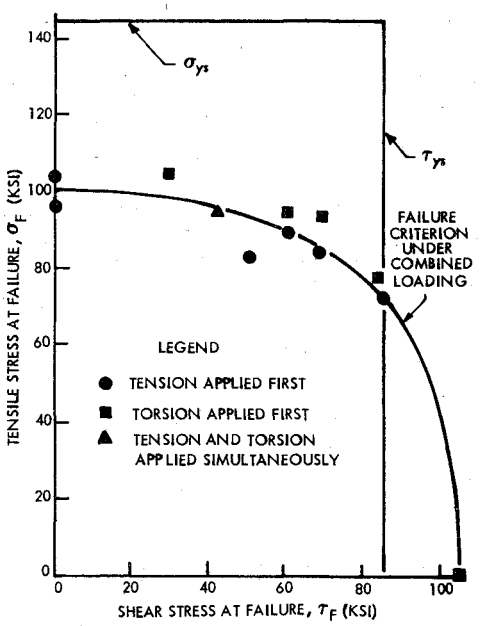

Fig. 8 Fracture results of titanium specimens subjected to tension and torsion ($a \approx 0.19$ in., $2c \approx 0.61$ in.).

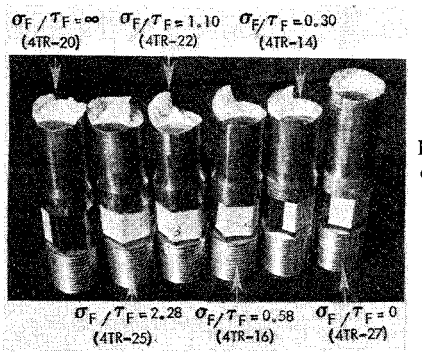

Fig. 9 Fracture surfaces of statically tested titanium specimens.

K_{Icr} and K_{IIIcr} are critical stress intensity factors for Mode I and Mode III, respectively.

Data of Figs. 5 and 6 of aluminum specimens, and Figs. 7 and 8 of titanium specimens are plotted in Figs. 10 and 11, respectively, as K_I/K_{Icr} (σ_F/σ_c) vs K_{III}/K_{IIIcr} (τ_F/τ_c). Figs. 10 and 11 also contain the probable fracture criterion and the lower bound of the fracture criterion for 4340 steel specimens subjected to combined Modes I and III loading.[11] These fracture criteria for 4340 steel were obtained from circumferentially notched round specimens subjected to tension and torsion loadings (Modes I and III), inclined surface flawed flat specimens subjected to tension (Modes I, II, and III) and surface flawed cylindrical specimens subjected to tension and torsion loadings (Modes I, II, and III). The probable fracture criterion for 4340 steel in Figs. 10 and 11 is described by the empirical equation[11]

$$(K_I/K_{Icr})^2 + (K_{III}/K_{IIIcr})^{4.75} = 1 \tag{3}$$

The lower bound of the fracture criterion for 4340 steel in Figs. 10 and 11 is described by the quadratic equation[11]

$$(K_I/K_{Icr})^2 + (K_{III}/K_{IIIcr})^2 = 1 \tag{4}$$

When data points with high shear stresses applied first to the specimens are neglected, results in Fig. 10 show that the fracture results of 2219-T87 aluminum specimens are well described by the fracture criterion of 4340 steel under combined Modes I and III given by Eq. (3). The suggested Eq. (3) does not seem to be applicable to cases when shear stress

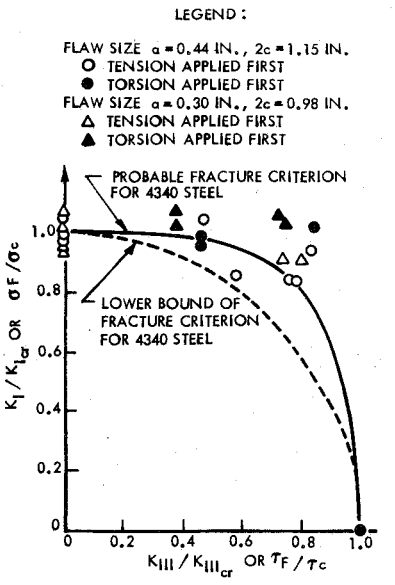

Fig. 10 K_I/K_{Icr} vs K_{III}/K_{IIIcr} for aluminum specimens subjected to tension and torsion.

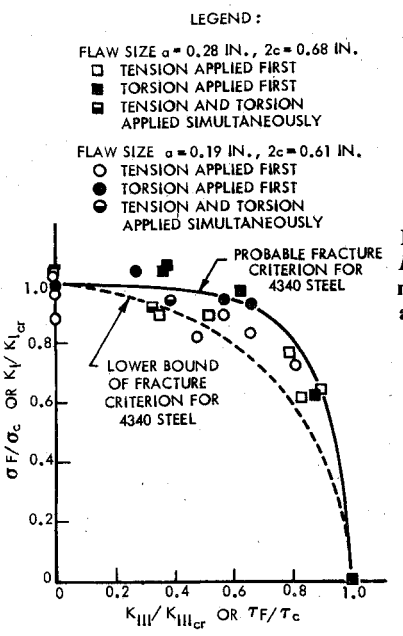

Fig. 11 K_I/K_{Icr} vs K_{III}/K_{IIIcr} for titanium specimens subjected to tension and torsion.

higher than 30 ksi due to torsion is applied first. The fracture criterion of 4340 steel given by Eq. (3) describes the combined mode results of titanium fairly well.

From the results of aluminum, titanium, and steel and combined Modes I and III results of 7075-T651 aluminum of Ref. 4 (results not shown here), it can be concluded that the lower bound of the fracture criterion under combined Modes I and III loading can be well described by Eq. (4). This suggests that the failure criterion given by Eq. (4) is very likely applicable to other materials where flaws are subjected to Modes I and III crack surface displacements. Strain energy density factor theory[8] also predicts that the fracture criterion under combined Mode I-III loading is a quadratic equation of K_I and K_{III}.

For pure torsion specimens of aluminum and titanium, the gross shear stress at the surface of the specimen (where it was maximum) was higher than the calculated shear yield strength of the material. This may have an effect on the fracture criterion. If Mode I experimental results of surface flaws in the presence of plastic yielding[13,14] are used for the interpretation of the above results of pure torsion, it would indicate that the shear stress at failure under elastic conditions would be slightly higher. Thus, ratios K_{III}/K_{IIIcr} would be

slightly smaller than those shown in Figs. 10 and 11, and would have a small effect on the failure criterion.

Cyclic Tests

For the sake of brevity, detailed test results of cyclic tests conducted on 36 surface flawed cylindrical specimens of aluminum and titanium are not shown here, but are described in Ref. 12. Approximate flaw sizes and ratios of applied tensile stress to shear stress σ/τ are shown in Table 3. Some of the aluminum and titanium specimens were fatigued under pure tensile stresses. Maximum cyclic tensile stresses were X percent (approximately 90%, 80%, and 70%) of the static failure stresses of the corresponding flaw size and material. Some of the aluminum and titanium specimens were fatigued under synchronously applied tensile and shear stresses. The ratios of applied tensile stress to shear stress, σ/τ, were generally either 2 or 1. Maximum cyclic tensile and shear stresses were X per cent (approximately 90%, 80%, and 70%) of the static fracture tensile and shear stresses of the corresponding σ/τ ratio, flaw size, and material. As seen from Figs. 5 and 8, the static tensile stresses at fracture for these two ratios of σ/τ were at least greater than 80% of the static tensile fracture stresses under pure tension for the corresponding flaw sizes. Maximum cyclic shear stresses for the aluminum and titanium specimens cycled under pure torsion were between 60-75% of the static fracture shear stresses for corresponding flaw size and material.

As previously mentioned, for the cyclic tests under combined tensile and shear stresses at a given σ/τ ratio, each of the maximum cyclic tensile and shear stresses was set at a percentage X of the corresponding static tensile and shear failure stresses given by Figs. 5-8. Fatigue tests of surface flawed specimens[15-19] have shown that, when critical flaw size is less than one-half of the specimen thickness, the number of uniform loading cycles (at a given cyclic stress ratio) required to grow a flaw from some initial flaw size to the critical flaw size is dependent primarily on the initial maximum stress intensity factor, K_{Ii}, applied at the tip of the flaw. K_{Ii} is the stress intensity factor based on the initial flaw dimensions and the maximum cyclic stress. Consequently, cyclic lives for precracked specimens at a given cyclic stress ratio are often primarily a function of the ratio K_{Ii}/K_{Icr}. This ratio is equivalent to the ratio of the maximum cyclic stress to the static fracture stress of the specimen with the same flaw size. Thus, K_{Ii}/K_{Icr} is the same as X defined before. Hence, an analysis was undertaken to compare the cyclic lives for combined tension and shear tests with those obtained for pure tension tests of surface flawed specimens in which the ratio of initial to critical stress intensity factors K_{Ii}/K_{Icr} was equal to X.[19]

As shown in Ref. 12, the critical flaw size was less than 0.4D for all but one of the cyclic tests of aluminum and titanium specimens. Data of cyclic tests of aluminum and titanium specimens are shown in Figs. 12 and 13, respectively, as X vs number of cycles to failure on a semilog plot where number of cycles to failure are plotted on a logarithmic scale. Since K_{Ii}/K_{Icr} or X vs cycles to failure data for beta processed 6A1-4V STA titanium is not available, data for alpha-beta processed 6A1-4V STA titanium from Ref. 19 is shown in Fig. 13. Both these materials have nearly the same fracture toughness. Also, crack growth rates are nearly the same for beta and alpha-beta processed titanium alloys.[20]

The curves shown in Figs. 12 and 13 were obtained from the data given in Tables 14 and 17 and 36-38 of Ref. 19, respectively. It was assumed that when $X=K_{Ii}/K_{Icr}$ is unity, application of one cycle will cause fracture. In constructing the curve in Fig. 12, only data from tests cycled to failure or cycled to very near to failure were used. For constructing the curve in Fig. 13, data of all tests were used, as there were only three specimens that were either cycled to failure or cycled very near to failure. The method used is the same as discussed

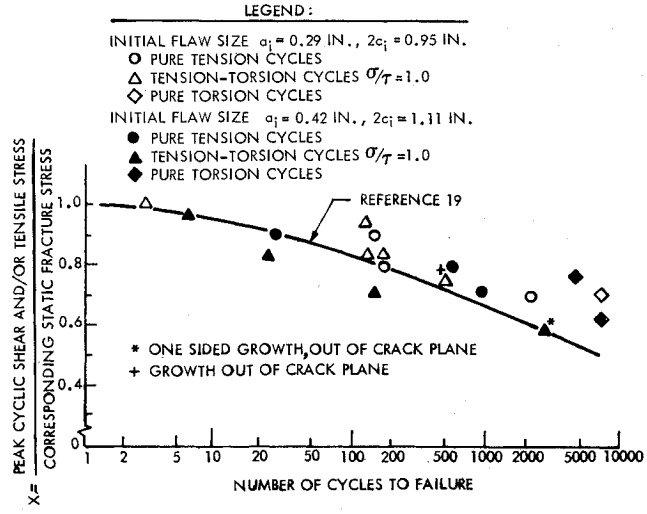

Fig. 12 Correlation between X and cycles to failure for aluminum specimens.

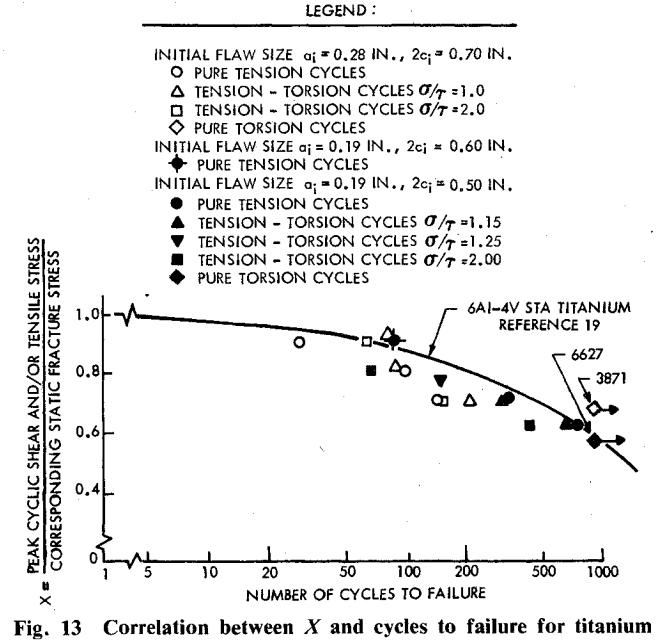

Fig. 13 Correlation between X and cycles to failure for titanium specimens.

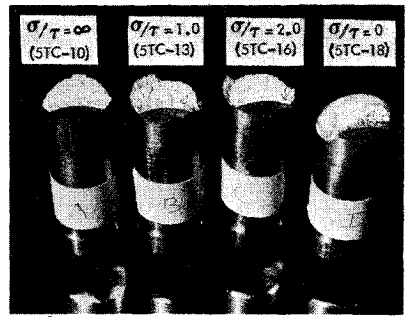

Fig. 14 Fracture surfaces of titanium specimens subjected to cyclic tensile and torsional loadings.

in Ref. 19. In constructing the curve in Fig. 13, emphasis was placed on the data of these three tests and the additional point located at $X=1$ and cycles to failure = 1. Data from tests that were not cycled to failure were adjusted in the following way. Two parallel lines for ordinates X given by K_{If}/K_{Icr} (where K_{If} is the stress intensity factor based on the flaw dimensions at the end of cyclic test) and K_{Ii}/K_{Icr} were first drawn. The abscissas were selected so that the difference between the two values was equal to the number of cycles applied during the

test and so that all data could be represented as closely as possible by a single curve. A single curve representation of the curve has been shown to be appropriate by many previous investigators.[15-19]

As seen from Ref. 20, a scatter factor of 2 in the crack growth rate at a given K, and hence in the cyclic life, is quite common for tests under pure tension for many materials. In view of this, results of Figs. 12 and 13 show that cyclic lives for combined tension and shear tests at a given X for ratios of $\sigma/\tau \geq 1$ compare reasonably well with cyclic lives for the surface flawed specimens subjected to pure tension at X. Figs. 12 and 13 show that the actual cyclic life for pure torsion specimens is about an order of magnitude greater than the cyclic life predicted from specimens subjected to pure tension. From the above limited results it may be concluded that cyclic lives for cracked specimens under combined tension and shear stresses of $\sigma/\tau \geq 1$ can be reasonably predicted from the cyclic lives of the surface flawed specimens subjected to pure tension. However, this requires a knowledge of factor X which, in turn, requires a knowledge of static fracture stresses.

Results of Figs. 12 and 13 show that, for the same value of X, cyclic lives for the specimens fatigued under pure tension stresses were significantly less than the cyclic lives for the specimens fatigued under pure shear stresses. X, here is $K_{\text{I}i}/K_{\text{Icr}}$ or $K_{\text{III}}/K_{\text{IIIcr}}$, depending upon tension or torsion loading. Results thus indicate that, in these tests, at any given value of X, fatigue crack propagation rates for tension stresses were higher than those for shear stresses.

Figure 14 shows the fracture surfaces of four specimens of titanium fatigued under four different ratios of σ/τ. As seen from the photograph in Fig. 14, the flaw growth in specimens fatigued under pure tensile stresses ($\sigma/\tau = \infty$) and combined tensile and shear stresses ($\sigma/\tau = 2$ and $\sigma/\tau = 1$) was nearly in the plane of the flaw. In fact, flaw growth in all specimens except specimens 5TC-9 ($\sigma/\tau = 0$), 5TC-18 ($\sigma/\tau = 0$), and 5TC-15 ($\sigma/\tau = 1.0$) was nearly in the plane of the crack.[12] Specimens 5TC-9, 5TC-18, and 5TC-15 were the only ones where fracture occurred while cycling.[12] In these three specimens also (as seen for specimen 5TC-18 from the photograph in Fig. 14), the initial flaw growth was nearly in the plane of flaw. Thus, it seems that the flaw grew out of its plane largely during the last cycles prior to fracture.

Conclusions

On the basis of examinations of the fracture surfaces, it was concluded that fractures in surface flawed cylindrical specimens subjected to combined Mode I-II-III crack surface displacements originated at or near the point of maximum crack depth where the constraint to crack tip deformation is maximum and only Mode I-III conditions existed.

Results obtained so far show that the failure criterion for 2219-T87 aluminum, 6A1-4V βSTA titanium and high strength 4340 steel under combined Mode I and III crack surface displacements can be adequately described by the single empirical equation of $K_{\text{I}}/K_{\text{Icr}}$ and $K_{\text{III}}/K_{\text{IIIcr}}$ given by Eq. (3). The results show that an applied tearing mode stress intensity factor K_{III}, less than 70% of K_{IIIcr}, has little effect (less than 20% of K_{Icr}) on the opening mode stress intensity factor K_{I} at which facture occurs. Similarly, the application of K_{I} up to about 70% of K_{Icr} has little effect (less than 20% of K_{IIIcr}) on the K_{III} at which fracture occurs.

The lower bound of the fracture criterion under combined Mode I and III loading for the aforementioned three materials and 7075-T651 aluminum is well described by the quadratic equation of $K_{\text{I}}/K_{\text{Icr}}$ and $K_{\text{III}}/K_{\text{IIIcr}}$ given by Eq. (4). This suggests that the failure criterion given by Eq. (4) is very likely applicable to other materials where flaws are subjected to Mode I and III crack surface displacements.

Cyclic lives for surface flawed cylindrical specimens subjected to combined tension and torsion with $\sigma/\tau \geq 1$ can be reasonably predicted from the cyclic lives of the surface flawed specimens subjected to pure tension and the static fracture criterion for the same specimen-flaw-configuration under combined tension and torsion.

References

[1] Erdogan, F. and Sih, G. C., "On the Crack Extension in Plates under Plane Loading and Transverse Shear," *Journal of Basic Engineering*, Vol. 85, Dec. 1963, pp. 519-527.

[2] Wu, E. M., "Application of Fracture Mechanics to Anisotropic Plates," *Journal of Applied Mechanics*, Vol. 89, Dec. 1967, pp. 967-974.

[3] Iida, S. and Kobayashi, A. S., "Crack Propagation Rate in 7075-T6 Plates under Cyclic Tensile and Transverse Shear Loadings," *Journal of Basic Engineering*, Vol. 91, Dec. 1969, pp. 764-769.

[4] Wilson, W. K., "On Combined Mode Fracture Mechanics," Research Report 69-1E7-FMECH-R1, June 1969, Westinghouse Research Labs., Pittsburgh, Pa.

[5] Pook, L. P., "Effect of Crack Angle on Fracture Toughness," *Engineering Fracture Mechanics*, Vol. 3, Oct. 1971, pp. 205-218.

[6] Roberts, R., and Kibler, J. J., "Mode II Fatigue Crack Propagation," *Journal of Basic Engineering*, Vol. 93, Dec. 1971, pp. 671-680.

[7] Liu, A. F., "Crack Growth and Failure of Aluminum Plate under In-Plane Shear," AIAA Paper 73-253, 1973, Washington, D.C.

[8] Sih, G. C., "Introductory Chapter: A Special Theory of Crack Propagation," *Methods of Analysis and Solutions of Crack Problems*, G. C. Sih, ed., Noordhoff International Publishing, Leyden, 1972.

[9] Sih, G. C. and MacDonald, B., "What the Designer Must Know about Fracture Mechanics," Applications of Fracture Mechanics to Engineering Problems, Lehigh University Report IFSM 72-23, Nov. 1972, Bethlehem, Pa.

[10] Palaniswamy, K. and Knauss, W. G., "Propagation of a Crack under General In-Plane Tension," *International Journal of Fracture*, Vol. 8, March 1972, pp. 114-117.

[11] Shah, R. C., "Fracture under Combined Modes in 4340 Steel," Fracture Analysis, ASTM Special Technical Publication 560, 1974, pp. 29-52.

[12] Shah, R. C., "Effects of Proof Loads and Combined Mode Loadings on Fracture and Flaw Growth Characteristics of Aerospace Alloys," CR-134611, March 1974, NASA.

[13] Masters, J. N., Haese, W. P., and Finger, R. W., "Investigation of Deep Flaws in Thin-Walled Tanks," CR-72606, Dec. 1969, NASA.

[14] Masters, J. N., Bixler, W. D. and Finger, R. W., "Fracture Characteristics of Structural Aerospace Alloys Containing Deep Surface Flaws," CR-134587, Dec. 1973, NASA.

[15] Tiffany, C. F., Lorenz, P. M., and Hall, L. R., "Investigation of Plane Strain Flaw Growth in Thick-Walled Tanks," CR-54837, Feb. 1966, NASA.

[16] Tiffany, C. F., Lorenz, P. M., and Shah, R. C., "Extended Loading of Cryogenic Tanks," CR-72252, July 1967, NASA.

[17] Hall, L. R. and Shah, R. C., "On Plane Strain Cyclic Flaw Growth Rates," *Engineering Fracture Mechanics*, Vol. 3, Aug. 1971, pp. 169-189.

[18] Tiffany, C. F., "Fracture Control of Metallic Pressure Vessels," NASA Special Publication 8040, May 1970.

[19] Hall, L. R. and Bixler, W. D., "Subcritical Crack Growth of Selected Aerospace Pressure Vessel Materials," CR-120834, Dec. 1972, NASA.

[20] "Damage Tolerant Design Handbook—Compilation of Fracture and Crack Growth Data for High-Strength Alloys," Metals and Ceramics Information Center Rept. MCIC-HB-01, 1973, Columbus, Ohio.